Direct and indirect noise generated by entropic and compositional inhomogeneities

Erwan O. Rolland*, Francesca De Domenico, Simone Hochgreb
Department of Engineering
University of Cambridge
Cambridge, CB2 1PZ
United Kingdom

Flow disturbances are generated inside a duct via pulsed injection of helium into a flow of air. This leads to the generation of an acoustic pulse (direct noise), as well as the production of entropic and compositional inhomogeneities which are convected with the mean flow. As these inhomogeneities are convected through a choked nozzle, they generate indirect noise. The resulting acoustic pressure fluctuations are measured experimentally using pressure transducers upstream of the nozzle. Insight obtained from theoretical models and a time-delay analysis can be used to isolate and extract the contributions of direct and indirect noise in the experimental signal. These results are directly compared to existing one-dimensional direct and indirect noise models. The experimental measurement of indirect noise is found to be in good agreement with the theoretical models for entropy noise and compositional noise for a compact one-dimensional isentropic nozzle.

Nomenclature

M Mach number [-]
P acoustic wave amplitude [-]
R acoustic reflection coefficient amplitude [-]
T temperature [K]
Y mass fraction [-]
Z mixture fraction [-]
c sound speed [m.s^{-1}]
c_p specific heat capacity [J.K^{-1} kg^{-1}]
g gibbs free energy [J.kg^{-1}]
$\dot{m}$ mass flow rate [g.s^{-1}]
p pressure [Pa]
s specific entropy [J.K^{-1} kg^{-1}]
u velocity [m.s^{-1}]
$\mathcal{L}$ acoustic dissipation coefficient [-]
γ heat capacity ratio [-]
ρ density [kg.m^{-3}]
ξ compositional wave amplitude [-]
σ entropy wave amplitude [-]
Φ_m mass flux perturbation [kg.m^{-2}.s^{-1}]
Φ_M momentum flux perturbation [kg.m^{-1}.s^{-2}]
Φ_e energy flux perturbation [J.m^{-2}.s^{-1}]
Φ_Z mass fraction perturbation [-]
φ_m normalized mass flux perturbation [-]
φ_M normalized momentum flux perturbation [-]
φ_e normalized energy flux perturbation [-]
φ_Z normalized mass fraction perturbation [-]
Ψ chemical potential function [-]
$(\cdot)_{\sigma/\xi}$ entropic/compositional noise
$(\cdot)_{d/i}$ direct/indirect noise
$(\cdot)_{air}$ relating to the air flow
$(\cdot)_{He}$ relating to the helium flow
$\bar{(\cdot)}$ mean component
$(\cdot)'$ fluctuating component
$(\cdot)^{\pm}$ forward or backward propagating

1 Introduction

Combustion noise is at the heart of several efforts to reduce aircraft emissions. First, as large reductions in jet and fan noise have been achieved, combustion noise emanating from the aero-engine is now a major contributor to the overall noise emitted by an aircraft. Parallel to this, the desire to reduce harmful pollutant emissions (such as NO_x) has led to the development of new lean-burn engines. However, these engines are particular susceptible to thermoacoustic instabilities [1], which can be triggered by combustion noise, and have a dramatic effect on engine performance. In this context, the development of a thorough understanding of combustion noise is an essential step in view of meeting future aircraft emission targets.

Combustion noise is comprised of direct and indirect noise [2]. The unsteady combustion process generates acoustic waves, known as direct noise, as well as convected flow disturbances, such as entropic, vortical or compositional inhomogeneities. These disturbances are quiescent by themselves, but if they are accelerated or decelerated (both of

*Address all correspondence to this author: eor21@cam.ac.uk

which are the case downstream of a gas turbine combustor), they generate indirect noise [3–5]. This noise propagates both downstream, where it contributes to overall aircraft noise, and upstream into the combustor, where it may bring about a thermoacoustic instability [6].

Indirect noise generated by the acceleration of deceleration of entropy disturbances ('entropy noise') was first investigated analytically in the 1970's [3, 7, 8]. However, experimental measurement of this effect has proved hard to achieve, not least due to the difficulty of separating direct and indirect noise, which are highly correlated [9].

Given the difficulty of separating direct and indirect noise inside a combustor, several experiments have attempted to study the indirect noise mechanism in a simplified situation, by generating entropy or vorticity waves artificially [10–15]. In the Entropy Wave Generator (EWG) experiment conducted at the German Aerospace Center (DLR) [12], an entropy wave was generated using a heating grid (leading to direct noise), convected through a duct, and accelerated through a converging-diverging nozzle (leading to indirect noise). The resulting acoustic pressure fluctuations were measured downstream of the nozzle, operated both in the subsonic and supersonic regimes.

The DLR experiment led to a series of analytical and numerical investigations aiming to explain its results [16–21]. These works indicate that the acoustic reflections downstream of the nozzle have a large effect on the measured acoustic signal [17, 22]. As a result, definitive conclusions regarding the indirect noise amplitude cannot be drawn from the experiment without precise knowledge regarding the acoustic boundary conditions of the system. These are particularly difficult to obtain at low frequencies, which the experiment is limited to due to the cooling time of the heating grid.

In addition, the direct and indirect noise signals appear to be 'merged', meaning that their relative contributions cannot be readily identified. In the subsonic case, it is not clear to which extent the measured pressure fluctuations correspond to indirect rather than direct noise [19–21].

Following the DLR experiment, another EWG was set up at Cambridge, in which acoustic fluctuations were measured upstream of the nozzle rather than downstream. Here, the direct and indirect noise were clearly separated in time, meaning that their contributions could be measured separately. Comparisons with low-order one-dimensional simulations [23] suggest that the entropy noise generated experimentally was considerably larger than predicted by the model developed by Marble and Candel [3]. However, these results are limited to low frequencies due to the heating grid used to generate the entropy waves.

In this paper, existing one-dimensional theoretical models for the generation of direct and indirect noise are presented. The experimental details are then described. Experimental results are presented, and compared to the one-dimensional analytical model. The implications of this comparison are then discussed.

2 Theoretical background

Flow fluctuations can be decomposed into acoustic, entropic, vortical and compositional disturbances. Flow variables of interest can be separated into a mean component (denoted with an over-bar) and a fluctuating component (denoted with a prime): $\alpha(x,t) = \bar{\alpha}(x) + \alpha'(x,t)$. In the linear approximation (i.e. $\alpha' \ll \bar{\alpha}$) these disturbances do not interact [24]. The acoustic, entropic and compositional disturbances can be thought of as waves of which the amplitudes are given by:

$$P^{\pm} \equiv \frac{1}{2}\left(\frac{p'}{\gamma\bar{p}} \pm \frac{u'}{\bar{c}}\right), \qquad \sigma \equiv \frac{s'}{c_p}, \qquad \xi \equiv Z'. \tag{1}$$

2.1 Direct noise

In the context of a combustor, direct noise refers to the noise directly generated by the unsteady heat release. This process is accompanied by the generation of flow disturbances, such as entropic and compositional inhomogeneities. In this paper, we call 'direct' the acoustic waves generated as a direct consequence of the localised unsteady heat release or fluid injection (as is the case in the present experiments). These waves would be generated even in a semi-infinite cylinder (where there is no acceleration or deceleration downstream of the localised perturbation).

Durán *et al.* [19] derived a simple one-dimensional model for the direct noise produced by a heating grid by considering the waves generated by a compact source of linear heat perturbations in the presence of a mean flow. By expressing this heat perturbation as a jump condition, they showed that such a source generates forward and backward acoustic waves, of which the amplitudes P_d^+ and P_d^- are a function of the mean Mach number $\bar{M}$, which is assumed to be constant across the jump, as well as the heat release perturbation. In addition, the heat perturbation leads to an entropy wave σ, which is convected with the mean flow. The assumption of compactness (i.e. the length of the source is negligible compared the wavelengths of interest) limits the applicability of this result to low-frequency perturbations.

Their approach can be extended to the case where the compact source induces perturbations of mass, momentum and energy flux, as well as mixture fraction (Φ_m, Φ_M , Φ_e and $\Phi_Z = Z'$ respectively) [23]. Implementing these perturbations as a jump condition on the linearised Euler equations, and considering that there are no impinging waves, the outgoing acoustic, entropic and compositional waves can be shown to be given by:

$$\begin{bmatrix} P_d^+ \\ P_d^- \\ \sigma \\ \xi \end{bmatrix} = \begin{bmatrix} \frac{1}{2}\frac{(\gamma-1)\bar{M}^3-\bar{M}^2}{\bar{M}+1} & \frac{1}{2}\frac{(1-\gamma)\bar{M}^3+\bar{M}^2}{\bar{M}+1} & \frac{1}{2}\frac{\bar{M}}{1+\bar{M}} & 0 \\ \frac{1}{2}\frac{(1-\gamma)\bar{M}^3-\bar{M}^2}{\bar{M}-1} & \frac{1}{2}\frac{(\gamma-1)\bar{M}^3+\bar{M}^2}{\bar{M}-1} & \frac{1}{2}\frac{\bar{M}}{1-\bar{M}} & 0 \\ (\gamma-1)\bar{M}^2-1 & (1-\gamma)\bar{M}^2 & 1 & -\bar{\Psi} \\ 0 & 0 & 0 & 1 \end{bmatrix} \begin{bmatrix} \varphi_m \\ \varphi_M \\ \varphi_e \\ \varphi_Z \end{bmatrix} \tag{2}$$

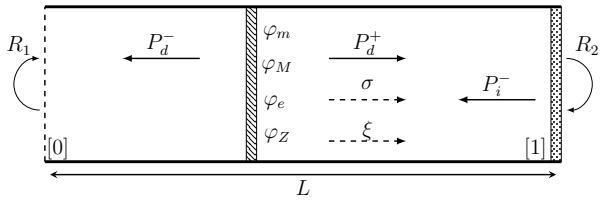

Fig. 1. Schematic of the direct acoustic wave, entropy wave and compositional wave generated at the jump location, and indirect acoustic wave generated at the outlet

where Ψ is defined in Eq. 7, φ_m, φ_M and φ_e are the normalized mass, momentum and energy flux changes at the interface, and φ_Z is the change in mixture fraction:

$$\varphi_m = \frac{\Phi_m}{\bar{\rho}\bar{u}}, \qquad \varphi_M = \frac{\Phi_M}{\bar{\rho}\bar{u}^2}, \qquad \varphi_e = \frac{\Phi_e}{\bar{\rho}\bar{u}C_p\bar{T}}, \qquad \varphi_Z = Z'. \tag{3}$$

A preliminary measure of the overall direct noise is given by the sum of the amplitudes of the forward and backward acoustic waves $P_d^+ + P_d^-$. The pressure fluctuation associated to the passage of those waves is given by $p' = \gamma\bar{p}(P_d^+ + P_d^-)$. If the mean Mach number is small ($\bar{M} \ll 1$), this can be approximated as:

$$p' \approx \gamma\bar{p}\frac{\bar{M}}{1-\bar{M}^2}\varphi_e \approx \frac{\gamma-1}{\bar{c}}\Phi_e \tag{4}$$

which shows that the amplitude of the direct noise is proportional to the energy flux perturbation Φ_e, and is nearly independent of the mean flow variables. In the context of this study, in which perturbations are generated by injecting helium radially into a main flow of air, the energy flux perturbation can be expressed as:

$$\Phi_e = \frac{\dot{m}_{He}}{A}c_{p,He}T_{He} \tag{5}$$

where A is the cross-sectional area of the main tube, and $\dot{m}_{He}$, $c_{p,He}$ and T_{He} are the mass flow rate, specific heat capacity and temperature of the injected helium. Combining Eqs. 4 and 5 shows that the pressure fluctuation resulting from the helium injection is expected to be proportional to the helium mass flow rate.

2.2 Indirect noise

Indirect noise is generated by the acceleration or deceleration of convected inhomogeneities, as is the case through a nozzle. Starting from the quasi-one-dimensional linearised Euler equations, Marble & Candel considered the case of a compact isentropic nozzle, deriving transfer functions of the response of such a nozzle to impinging perturbations [3]. The backward-propagating wave generated by an incoming entropy wave σ is given by:

$$\frac{P_\sigma^-}{\sigma} = -\frac{\bar{M}_2-\bar{M}_1}{1-\bar{M}_1}\frac{\bar{M}_1}{2+(\gamma-1)\bar{M}_1\bar{M}_2} \tag{6}$$

where $\bar{M}_1$ and $\bar{M}_2$ are the Mach numbers upstream and downstream of the nozzle respectively.

This approach was extended to a multi-component gas mixture by Magri *et al.* [5]. They introduced the chemical potential function of a mixture as Ψ:

$$\Psi = \frac{1}{c_p\bar{T}}\sum_{n=1}^{N} g_n(T,p)\frac{dY_n}{dZ} \tag{7}$$

where g_n and Y_n are the specific Gibbs free energy and mass fraction of one of N species. This study is concerned only with the case where the gas is a mixture of air and helium, for which the mixture fraction can be taken directly as the mass fraction of helium ($Z = Y_{He}$). The chemical potential function of a given mixture is dependent on pressure and temperature, and if the mixture is accelerated through a nozzle, its value changes accordingly (from Ψ_1 to Ψ_2). This change in chemical potential across the nozzle drives the generation of indirect noise - referred to as 'compositional noise' here. The amplitudes of the acoustic waves generated downstream of the nozzle due to an impinging compositional wave are derived by Ihme [25]. The amplitude of the upstream backward-propagating acoustic wave generated by an incoming compositional perturbation ξ is given by:

$$\begin{aligned}\frac{P_\xi^-}{\xi} = &\frac{(\gamma-1)(\Psi_1-\Psi_2)[2+(\gamma-1)\bar{M}_1^2]\bar{M}_1\bar{M}_2}{(\gamma-1)(\bar{M}_1-1)(\bar{M}_1+\bar{M}_2)[2+(\gamma-1)\bar{M}_1\bar{M}_2]} \\ &+\frac{\bar{M}_1[2(\Psi_1-\Psi_2)+(\gamma-1)(\Psi_1\bar{M}_2^2-\Psi_2\bar{M}_1^2)]}{(\gamma-1)(\bar{M}_1-1)(\bar{M}_1+\bar{M}_2)[2+(\gamma-1)\bar{M}_1\bar{M}_2]}\end{aligned} \tag{8}$$

The limit case of a choked or supersonic nozzle is obtained by considering the case where $\bar{M}_2 = 1$. The total indirect noise is then a combination of the entropy and compositional noise: $P_i^- = (P_\xi^-/\xi)\xi + (P_\sigma^-/\sigma)\sigma$

2.3 Reverberation

Reverberation occurs when a given acoustic signal is repeatedly reflected within a short period of time, causing a large number of reflections to build up, and modifying the acoustic pressure.

For example, one can consider the one-dimensional case of a cavity: two walls separated by a distance L. A square acoustic pulse is generated at the first wall, from $t = 0$ to $t = t_p$. The acoustic wave thus generated will propagate towards the other wall at the speed of sound $\bar{c}$. Once it reaches the wall, it will be reflected back towards the first wall, get reflected towards the second wall, get reflected towards the first wall once again etc. If the time taken for an acoustic

wave to be reflected back to its original position $T = 2L/\bar{c}$ is smaller than the duration of the acoustic pulse t_p, then the successive reflections will be superimposed with the acoustic wave being simultaneously generated. As a result, the acoustic pressure will 'build-up' throughout the duration of the acoustic pulse.

Owing to limitations in the experimental set-up, Entropy Wave Generators such as the one presented in this study often operate at very low frequencies (typically less than 10 Hz). If the boundaries of the EWG are highly reflective, this may lead to reverberation, whereby the sound pressure in the EWG 'builds-up' as a given acoustic wave is repeatedly reflected while the sound source is still active.

The reverberation process modifies both the shape and amplitude of the measured acoustic pressure, and affects direct and indirect noise differently. As shown in detail [23], the pressure fluctuation resulting from the reverberation of a square direct or indirect acoustic pulse is the sum of the terms of a geometric series, and can be approximated as:

$$\left.\frac{p'}{\gamma\bar{p}}\right|_d (0 < t \leq t_p) \approx (P_d^+ + P_d^- R_1)(1+R_2)\frac{1-(R_1R_2)^{\lfloor \frac{t+T}{T} \rfloor}}{1-R_1R_2} \tag{9}$$

$$\left.\frac{p'}{\gamma\bar{p}}\right|_i (\tau_c < t \leq \tau_c + t_p) \approx P_i^-(1+R_1)\frac{1-(R_1R_2)^{\lfloor \frac{t-\tau_c+T}{T} \rfloor}}{1-R_1R_2} \tag{10}$$

where $T = 2L/\bar{c}$ is the acoustic time-scale of the system, $\tau_c = L_c/\bar{u}$ is the convective time delay, and R_1 and R_2 are the acoustic reflection coefficients at the inlet and outlet of the system. If R_1 and R_2 are positive, the reverberation 'amplifies' the original acoustic signal, and the pressure reaches a maximum $p'/\gamma\bar{p}|_{max}$ just as the acoustic source is switched off at $t = t_p$. The acoustic signal then decays as acoustic power is lost due to the imperfect reflections at the edges of the system. The decay is given by:

$$\left.\frac{p'}{\gamma\bar{p}}\right| (t > t_p) \approx \left.\frac{p'}{\gamma\bar{p}}\right|_{max} (R_1R_2)^{\lfloor \frac{t-t_p}{T} \rfloor} \tag{11}$$

If the only acoustic sources in the system are direct and indirect noise, then the acoustic pressure can be taken as the sum of direct and indirect noise: $p'/\gamma\bar{p}(t) = p'/\gamma\bar{p}|_i(t) + p'/\gamma\bar{p}|_d(t)$ owing to the superposition principle.

The equations above can be applied to the example of a one-dimensional cavity of width $L = 1$ m, where the walls have reflection coefficients $R_1 = 1$ and $R_2 = 0.95$. We consider a square acoustic pulse of duration $t_p = 100$ ms and of amplitude $P^+ = 5 \times 10^{-4}$ (corresponding to a pressure fluctuation of roughly 70 Pa in air at atmospheric conditions). At atmospheric conditions, we have $T \approx 5.8$ ms $\ll t_p$, and reverberation occurs. The resulting acoustic pressure is shown in Fig. 2, along with the square acoustic pulse (without acoustic reflections) for reference.

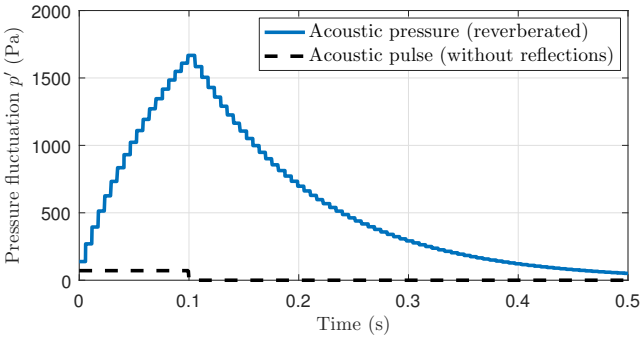

Fig. 2. Acoustic pressure resulting from a reverberated square acoustic pulse in a one-dimensional cavity

Clearly, the reverberated pressure is much higher than would be expected if no acoustic reflections occurred - in this example the peak of the acoustic signal is amplified by a factor of roughly 20. The acoustic pressure rises while the acoustic source is active (from $t = 0$ to $t = t_p$). If the source is kept active for long enough, the acoustic pressure will eventually converge towards a limit, which is a balance between the acoustic energy being generated, and the losses at walls (since $R_2 < 1$). The discontinuities in the pressure signal correspond to the successive reflections of the square wave, and are spaced by a time delay T. Once the source is switched off at $t = t_p = 100$ ms, the acoustic pressure decays as the acoustic energy slowly leaves the system.

3 Experimental details

The experiment is conducted using the Cambridge Entropy Wave Generator rig, in a configuration similar to that described in [14]. The aim of this setup is to detect and separate artificially generated direct and indirect noise. The main difference from previous experiments is that the entropy wave is now generated by injecting a fluctuating mass flow of helium into a main flow of air, which also generates a compositional wave. The tube is terminated with a choked nozzle (reaching a Mach number of 1), with a throat diameter of 4 mm. The nozzle has a linear geometric profile with a length of 40 mm, and can be considered acoustically compact for the perturbation frequencies of concern in this study.

3.1 Experimental Setup

The Cambridge Entropy Wave Generator rig is shown schematically in Fig. 3. Air flows through a straight tube of length L at a controlled rate. A secondary flow of helium is dispensed into the flow radially at some distance L_c upstream of the outlet. The gas mixture exits via an outlet, which consists of a choked nozzle. Dynamic pressure measurements are carried out using flush mounted pressure transducers.

The primary air flow is supplied via the laboratory's compressed-air delivery system, and fed through a 250 L tank to dampen out undesirable acoustic oscillations. The flow is controlled using a pressure regulator and a mass flow controller (Alicat MCR500), and connected to the straight

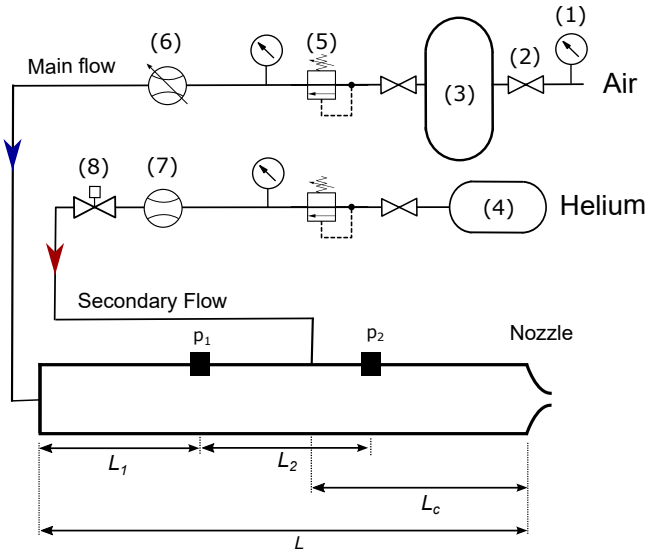

Fig. 3. Experimental setup: flow circuit with (1) pressure indicators, (2) valves, (3) air tank, (4) helium tank, (5) pressure regulator, (6) mass flow controller, (7) mass flow meter, (8) fast solenoid valve

tube via a 12 mm flexible PVC hose. The tube itself consists of a PVC tube with a diameter of 42.6 mm.

The secondary flow consists of helium (>99.996% purity) delivered at room temperature by a 200 bar bottle fitted with a 2-stage pressure regulator. The helium is injected radially into the main tube using a fast-switching solenoid valve (ASCO Numatics HSM2L7H50V). Given that the valve orifice size is fixed, the amount of injected gas can be varied by modifying the pressure upstream of the solenoid valve, which is achieved using a pressure regulator. The mass flow rate and temperature of the injected gas is monitored using a mass flow meter (Alicat MCR250). The valve is connected to the straight duct via a 0.1 m length of flexible tubing with a 2 mm inner diameter.

3.2 Pressure Measurements

Acoustic pressure measurements are carried out using a pair of Kulite XTE-190(M) piezoresistive pressure transducers, flush mounted at distances L_1=0.8 m and L_2=1.2 m of the inlet. The absolute pressure is recorded using a Kulite XT-140M piezoresistive pressure transducer, which is mounted at a distance L_2 from the inlet. The transducer signals are amplified using a Flyde FE-379-TA amplifier, and acquired using a NI-2090 DAQ box connected to a NI PCI-5259 card. The signal is sampled at 8192 Hz with a 16-bit resolution.

The raw pressure signal is phase-averaged for 100 helium pulses, and filtered to eliminate oscillations at 50 Hz (power frequency signal), as well as frequency components above 400 Hz (far above the frequencies of interest here).

3.3 Experimental configurations

For this study, 3 different experimental configurations (A, B and C) are examined, with 8 experimental cases in total. For each of these configurations, the mass flow rate of air flow rate is varied from 5.92 to 9.87 g.s^{-1}, at a temperature of 294 K on average. In all cases, the Mach number inside the tube is $\bar{M} = 0.0052$. In each case, helium is injected in pulses lasting $t_p = 100$ ms with a period of 4 s, at five different flow rates (0.027, 0.055, 0.082, 0.109, 0.136 g.s^{-1}), at a temperature of 296 K on average. Each test is repeated for 100 pulses.

In configuration A, the length of the tube is extended to L =62.6 m using 60 m of flexible tubing of an identical inner diameter. Given the very long length of this system, the acoustic time-scale ($T \approx 0.37$ s) is much larger than the pulse duration (100 ms), meaning that reverberation of the acoustic signal will not occur. Additionally, the convective distance L_c from the point of helium injection to the outlet is large, meaning that the convective time delay τ_c is much larger than the pulse duration, meaning that direct and indirect noise will not interact. These two factors enable the pressure transducers to measure the amplitudes of the direct noise waves resulting from the injection process. The transducers p_1 and p_2 measure $(1+R_1)P_d^-$ and $P_d^+ + R_1 P_d^-$ respectively. This configuration is designed to assess the validity of the direct noise model.

In configuration B, the length of the tube is L =1.6 m, corresponding to an acoustic time-scale of $T \approx 10$ ms, shorter than the pulse duration, meaning that reverberation occurs. The convective distance L_c from the point of helium injection to the outlet is much smaller than in configuration A, and direct and indirect noise can be expected to interact. This configuration is designed to examine the validity of the reverberation model.

Finally, in configuration C, the injector is placed at a small distance L_i=0.05 m upstream of the nozzle. The convective distance L_c from the point of helium injection to the outlet is extremely short, meaning that direct and indirect noise are generated simultaneously. In addition, dispersion and diffusion of the helium disturbance can be expected to be far less pronounced than in configurations A and B. This configuration is designed to verify the applicability of the indirect noise models.

A summary of the operating conditions for each of the 8 experimental cases is presented in Table 1.

4 Experimental results

4.1 Configuration A: Direct noise

In this configuration, transducers at locations p_1 and p_2 are used to measure the acoustic waves resulting from the helium injection. In a one-dimensional framework, the transducer p_1 upstream of the injection point measures the backward-propagating direct noise wave P_d^-. After a very short time (roughly $T_1 = 2L_1/c \approx 4$ ms), the wave is reflected at the inlet with an amplitude $R_1 P_d^-$. Since the reflection delay is much smaller than the pulse duration $t_p = 100$ ms, the transducer effectively measures the pressure fluctuation corresponding to the passage of a wave of amplitude $(1+R_1)P_d^-$. Similarly, the transducer p_2 measures the pressure fluctuation corresponding to $P_d^+ + R_1 P_d^-$; the resulting pressure trace is shown in Fig. 4.

Table 1. EXPERIMENTAL CASES WITH CONVECTIVE LENGTH, TUBE LENGTH, MEAN PRESSURE, AIR AND HELIUM MASS FLOW RATES.

Case	L_c [m]	L [m]	$\bar{p}$ [kPa]	$\dot{m}_{air}$ [g.s^{-1}]	$\dot{m}_{He}$ [g.s^{-1}]
A1	61.65	62.6	199.0	5.92	For each case: 0.027, 0.055, 0.082, 0.109, 0.136
A2	61.65	62.6	263.4	7.89	
B1	0.65	1.6	199.1	5.92	
B2	0.65	1.6	263.4	7.89	
B3	0.65	1.6	328.8	9.87	
C1	0.05	1.6	199.0	5.92	
C2	0.05	1.6	263.2	7.89	
C3	0.05	1.6	328.5	9.87	

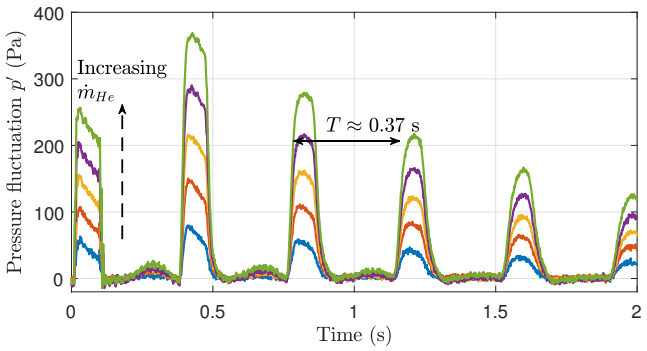

Fig. 4. Acoustic pressure p'_2 (case A2) as a function of time t for 5 different helium flow rates

The first pulse in Fig. 4 coincides with the valve pulse signal (from $t = 0$ to $t = 100$ ms), and corresponds to the direct noise generated by the helium injection. At intervals of $T = 2L/c$, this acoustic wave is reflected back to its original position, and measured once again. The fact that reflected signals are of the same sign as the original pulse show that the nozzle reflection coefficient R_2 is positive (as expected).

Given the amplitude of the first pulse $P_0 = (P_d^+ + R_1 P_d^-)$, the amplitude of the following pulse is roughly $P_1 = \mathcal{L} R_2 (1 + R_1) P_0$, where $0 < \mathcal{L} < 1$ is a loss coefficient due to acoustic dissipation in the tube. The amplitude of the following pulses are simply $P_2 = \mathcal{L} R_2 P_1$, $P_3 = \mathcal{L} R_2 P_2$, etc.

In the first acoustic pulse, the pressure fluctuation quickly reaches a maximum value, then decreases steadily until $t = t_p$ when it falls to to zero. This is consistent with the 1D direct noise model presented in Sec. 2 , which suggests that the acoustic pressure fluctuation is proportional to the injected mass flow rate of helium. Indeed, the helium mass flow rate is at a maximum when the solenoid valve is opened, and the pressure upstream of the valve is at its maximum. As the helium flows, the pressure upstream of the valve decreases from its original value too quickly for the pressure regulator to correct for, resulting in a lower acoustic pressure in the tube.

Finally, as the mass flow rate of injected helium $\dot{m}_{He}$ is increased, the acoustic pressure fluctuation increases. The measured pressure fluctuation corresponding to the direct noise pulse is plotted as a function of injected energy flux Φ_e in Fig. 5, and compared to the 1D acoustic model assuming $R_1 \approx 1$.

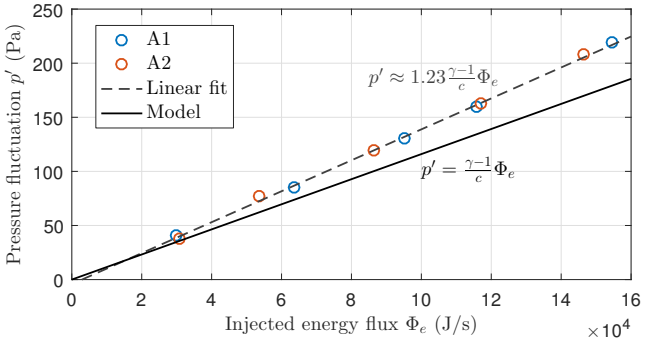

Fig. 5. Acoustic pressure pulse amplitude p'_2 as a function of injected energy flux Φ_e (cases A1 and A2), compared with the theoretical 1D direct noise model

The direct noise amplitude is consistently underestimated by the 1D theoretical model. However, the model correctly predicts the linear relationship between acoustic pressure and injected energy flux; they appear to be related by proportionality coefficient independent of the mean pressure. The apparent proportionality coefficient in the experimental results is 23% larger than predicted by the theoretical model.

The discrepancy between the theoretical direct noise model and the experimental results is not entirely surprising, as some sources of noise are not included in the theoretical model. Indeed, while the effects of mass, momentum and energy addition are taken into account, other aspects of the injection (formation of a jet, vorticity generation) are not considered since the model is 1D. Most importantly, the injected helium decelerates and depressurizes as it is adjusts to the the mean flow in the duct. These changes are accompanied by changes in the chemical potential function Ψ and Mach number, which drive the generation of entropic and compositional noise (see Eqs. 6 and 8). As such, the noise generated at the injection location is likely to be a sum of direct and indirect noise.

A corrected direct noise model can be adopted by correcting the theoretical model to match the experimental results. This is done by multiplying the output of the theoretical model by 1.23 (to match the proportionately coefficient). This 'experimental direct noise model' is used throughout the rest of the work, so that the mismatch here does not affect the rest of the analysis.

4.2 Configuration B: Reverberation

Unlike configuration A, the tube length L in configuration B is short enough for reverberation to occur. We also expect some indirect noise to be generated as the helium disturbance is convected through the nozzle. The acoustic pressure measurements for cases B1, B2 and B3 for a range of helium flow rates are shown in Fig. 6. As the helium mass flow rate is increased, the amplitude of the acoustic pressure fluctuation increases, which is consistent with cases A1 and A2. As a result, the acoustic signal is amplified (by a factor of roughly 20 compared to cases A1 and A2).

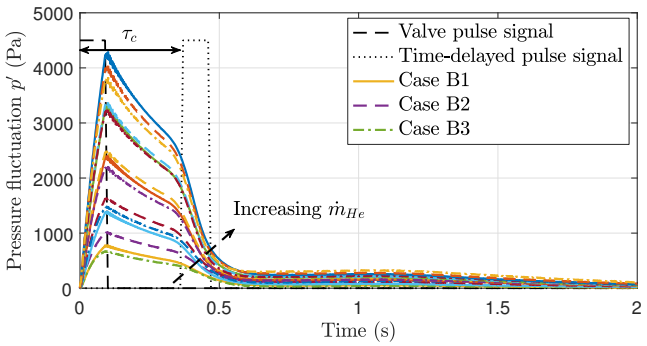

Fig. 6. Experimental acoustic pressure p'_2 (cases B1, B2, B3) as a function of time t for a range of helium flow rates

The aspect of the pressure signal can be explained by considering the pulse duration t_p and convective time delay τ_c. During the valve pulse signal (from $t = 0$ to $t = t_p = 100$ ms), the acoustic pressure rises continuously. This is due to the reverberation of the direct noise signal, and is consistent with Eq. 9. Once this acoustic source is switched off at $t = t_p$, the acoustic pressure decays exponentially, as suggested by Eq. 11. At $t = \tau_c$ (when the helium reaches the choked nozzle), there is a considerable change in slope in the pressure signal. Once the disturbance has been completely convected through he nozzle (at $t \approx \tau_c + t_p$), the signal appears to decay at a more moderate rate once again.

Based on this analysis, it is apparent that the acoustic signal visible from $t = 0$ to $t = \tau_c$ is entirely due to direct noise (or other noise accompanying the helium injection). Equation 11 shows how this signal is expected to decay as a function of the direct noise wave amplitudes P_d^+ and P_d^- (which can be obtained using the experimental direct noise model), the length of the system L, and the product of reflection coefficients R_1R_2. An estimation of R_1R_2 can be obtained by fitting the pressure signal predicted by Eq. 11 to the experimental signal, as shown in Fig. 7.

There is good agreement between the experimental signal and the direct noise reverberation decay model for $R_1R_2 = 0.983 \pm 0.2\%$ (the value ranges from 0.981 to 0.985 depending on the experimental case). The left hand side of Fig. 7 shows how that the decay rate is very sensitive to the value of R_1R_2, suggesting that our estimation of this value is likely to be precise. This result is consistent with the fact that a choked nozzle acts as a velocity node, and the mass flow

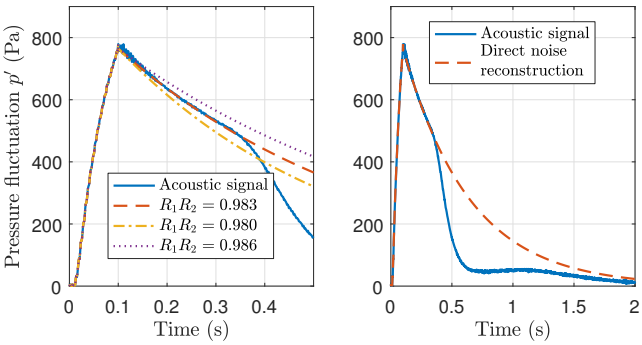

Fig. 7. Experimental acoustic pressure (case B1) and theoretical acoustic decay model as a function of time t for different values of R_1R_2 (left) and for $R_1R_2 = 0.983$ (right)

rate at the inlet is fixed, meaning that both R_1 and R_2 can be expected to be close to unity.

The decay model enables us to extrapolate the decay of the experimental signal for direct noise beyond $t = \tau_c$, at which the experimental signal becomes a combination of direct and indirect noise. As such, the direct noise measured experimentally can be 'reconstructed', as shown on the right-hand side of Fig. 7.

Using the superposition principle, we can now identify which portion of the measured acoustic pressure p' is not due to direct noise p'_d by subtraction. In our case, the only other source of noise is indirect noise p'_i, such that $p'_i = p' - p'_d$. As such, the indirect noise signal can be extracted from the experimental signal, as shown in Fig. 8.

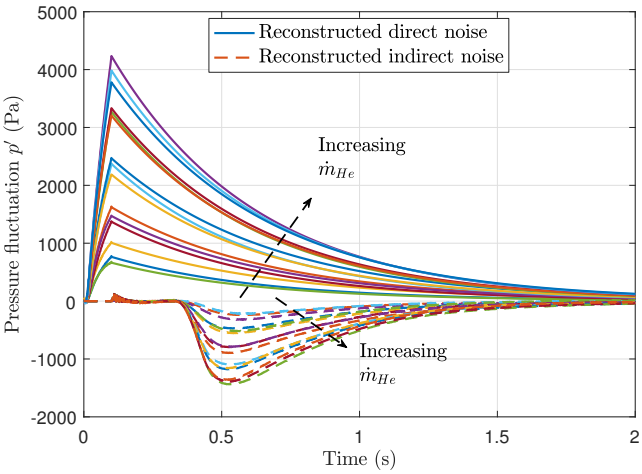

Fig. 8. Reconstructed experimental direct noise (p'_d) and indirect noise (p'_d) (cases B1, B2 and B3.

As expected, the indirect noise appears to start around $t = \tau_c$ in all cases. The magnitude of the indirect pressure increases continuously for roughly 100 ms (the pulse duration), following which it decays towards 0. The amplitude of the indirect noise increases with the mass flow rate of helium injected.

4.3 Configuration C: Indirect noise

Configuration C is similar to configuration B, except that the point of injection is now directly upstream of the nozzle, with a small convective time delay. As a result, one would expect direct and indirect noise to be almost completely merged. Since the tube length and reflection coefficients of the system are unchanged, the effect of reverberation should be identical to that in configuration B. The experimental measurement of the acoustic pressure for cases C1, C2 and C3 is plotted in Fig. 9.

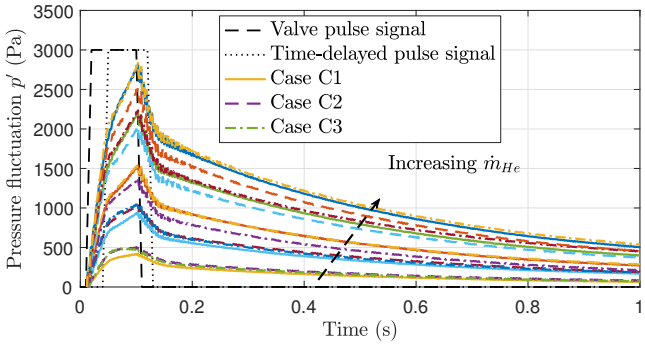

Fig. 9. Experimental acoustic pressure p'_2 (cases C1, C2, C3) as a function of time t for a range of helium flow rates

The peak pressure is lower than for the corresponding operating conditions in Configuration B. Indeed, the indirect noise (negative) and direct noise (positive) are now generated almost simultaneously, leading to destructive interference. From $t = 0$ to $t = \tau_c \approx 30$ ms, the pressure rises sharply due to the direct noise. Once the helium disturbance starts convecting through the nozzle at $t = \tau_c$, the slope of the acoustic pressure signal decreases (negative interference) As the valve is closed at $t = t_p = 100$ ms, the direct noise ceases, and the acoustic pressure starts to decrease. This decrease occurs faster once indirect noise is no longer generated from $t = \tau_c + t_p$ onwards.

Once again, the direct noise can be reconstructed using the reflection coefficient product $R_1 R_2$ measured in Sec. 4.2, and the indirect noise can be extracted from the experimental signal. These are plotted as a function of time in Fig. 10.

Unlike configuration B, the indirect noise signal extracted from the experimental data now starts closer to $t = 0$, owing to the shorter convective delay τ_c. The small differences in amplitude of the reconstructed direct noise in configurations B (Fig. 8) and C (Fig. 10) are due to the slight variations in the helium flow rates achieved for each experiment.

5 Theoretical results

5.1 Analytical model

The analytical formulas presented in 2 can be combined to provide a single theoretical model for the acoustic pressure resulting from the helium injection. This is shown diagrammatically in Fig. 11. The results of this model can be compared directly to the experimental results.The mass, momentum, energy and compositional fluctuations (φ_m, φ_M, φ_e and φ_Z) corresponding to the helium injection are known for the experimental cases. The direct noise model (shown in Eq. 2 and corrected as shown in section 4.1), can then be used to obtain values for the direct noise acoustic waves P_d^+ and P_d^-. The amplitudes of the entropy (σ) and compositional (ξ) waves generated by the injection of helium can also be obtained from Eq. 2. The indirect acoustic waves (P_σ^- an P_ξ^-) corresponding to these disturbances can be computed using the compact nozzle transfer functions shown in Eqs. 6 and 8. The reflection coefficients of the system R_1 and R_2 can be obtained from the experimental data as shown in section 4.2. The pulse length t_p and acoustic time scales of the system T and τ_c are known. These parameters can then be used in the reverberation model, obtaining separate signals for the direct noise (p'_d), entropy noise (p'_σ), and compositional noise (p'_ξ). The overall acoustic pressure fluctuation corresponds to the sum of these signals.

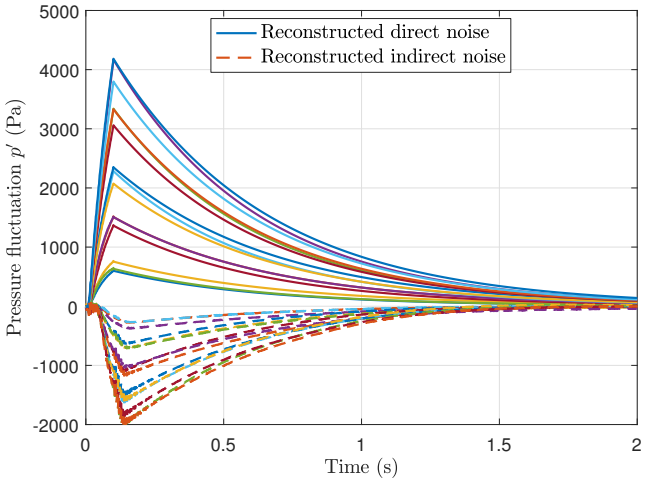

Fig. 10. Reconstructed experimental direct noise (p'_d) and indirect noise (p'_d) (cases C1, C2 and C3).

5.2 Results

The analytical results obtained for cases B1, B2 and B3 are shown in Fig. 12, along with the corresponding experimental signals for reference. The overall shape and trend of the acoustic pressure signal is correctly recovered by the analytical model. At first, the pressure rises sharply due to the direct noise, reaching a maximum at $t = t_p$. This peak is correctly reproduced by the analytical model. The direct noise then decays exponentially, identically to the experimental signal. Indirect noise is generated at $t = \tau_c$, and interacts de-constructively with the direct noise signal, as they are of opposite signs. In the experimental signal, this interaction results in a positive pressure 'plateau'. In the analytical result, this behaviour is recovered, although the 'plateau' is now close to 0 Pa; the direct and indirect noise appear to cancel out almost exactly. This suggests that the indirect noise is slightly over predicted compared to the experiment.

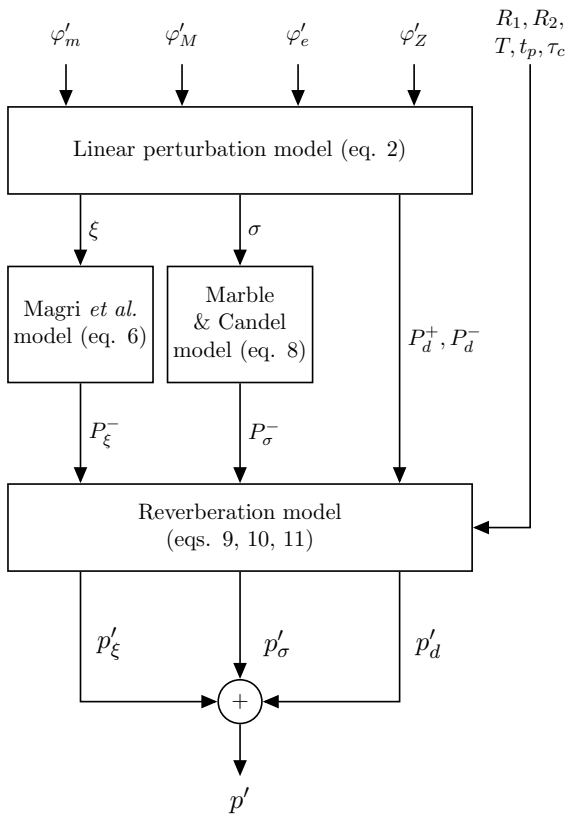

Fig. 11. Block diagram representing the equations composing the analytical model

Comparing Figs. 8 and 12 (right) confirms that the indirect noise is over-predicted. This is expected. Indeed, as the helium disturbance is convected from the injection point to the nozzle, one would expect for it to diffuse and disperse (due to the 2D velocity profile). As a result, the amplitude of the entropic and compositional fluctuations σ and ξ is expected to decrease, which would lead to a lower indirect noise signal. The diffusion and dispersion of the helium disturbance is not taken into account here, which partly explains this discrepancy. Furthermore, the indirect noise obtained analytically has a 'sharp' aspect: it rises very sharply towards a maximum peak value. This behavior is not present in the experimental reconstruction of the indirect noise signal, which appears to rise more 'smoothly'. Once again, this can be explained by the effect of convection on the helium disturbance. Indeed, while the helium pulse is assumed to be perfectly square in the analytical model, in reality the dispersion and diffusion processes smooth out the shape of the pulse, which can be expected to resemble a Gaussian once it reaches the nozzle.

The analytical results obtained for cases C1, C2 and C3 are shown in Fig. 13, along with the corresponding experimental signals for reference. Once again, the overall shape and trend of each signal is correctly predicted. Comparing Figs. 10 and 13 (right) shows that the indirect noise is once again slightly over-predicted (although less so than in cases B1, B2 and B3). This explains why the pressure peak predicted by the analytical model is slightly lower than in the experiment, as the over-estimation of indirect noise leads to a reduction in overall acoustic pressure. However, unlike cases B1, B2 and B3, the shape of the indirect noise signal is correctly predicted. This is due to the fact that the helium injection location is now directly upstream of the nozzle, and the convection distance $L_c = 0.05$m is too short for significant diffusion or dispersion to occur.

The indirect noise signal obtained analytically is the sum of entropy and compositional noise signals. Their contributions to the overall indirect noise are shown in Fig. 14 for cases C1, C2 and C3. The entropy noise is negative, while the compositional is positive. However, the entropy noise is more significant than the compositional noise in the cases presented here, so the overall indirect noise pressure signal is negative. Although this is not immediately apparent from observing the overall acoustic pressure signal for configuration C, this suggests that the entropy noise is actually more significant than the direct noise (though this is partially attenuated due to the compositional noise).

Figure 15 shows a comparison between the experimental and analytical results for the peak acoustic pressure for direct and indirect noise. The direct noise comparison is based on configuration B, in which the direct noise peak is not affected by the indirect noise (which is not the case configuration C). Conversely, the indirect noise comparison is based on configuration C, where the effect of convection between the valve and the nozzle does not need to be taken into account.

The direct noise comparison shows that there is very good agreement between the experimental and analytical results. The direct noise acoustic wave amplitudes are obtained directly from experimental measurements (cases A1 and A2), as explained in section 4.1. As shown in Fig. 11, the only model used to obtain the analytical results is then the reverberation model. As such, the agreement between the experimental results and the analytical results suggest that the reverberation model is accurately capturing the physics of the experiment correctly.

The indirect noise comparison shows a relatively good agreement between the experimental and analytical results. Notably, the experimental data shows that indirect noise pressure peak increases nearly linearly with the injected energy flux Φ_e, which is consistent with the analytical results. The difference between the analytical and experimental results is roughly 7%. Since the reverberation model appears to be accurate (based on the excellent agreement for the direct noise), this discrepancy is likely to be related to another part of the analytical model. As such, the error could be due to one of the nozzle transfer functions employed (Eqs. 6 and 8), and/or the entropy and compositional wave amplitudes computed using Eq. 2. Alternatively, the mismatch could be the result of an additional effect not accounted for in the theoretical model.

6 Conclusions

A series of experiments has been performed to quantify the amount of direct noise, entropy noise, and compositional

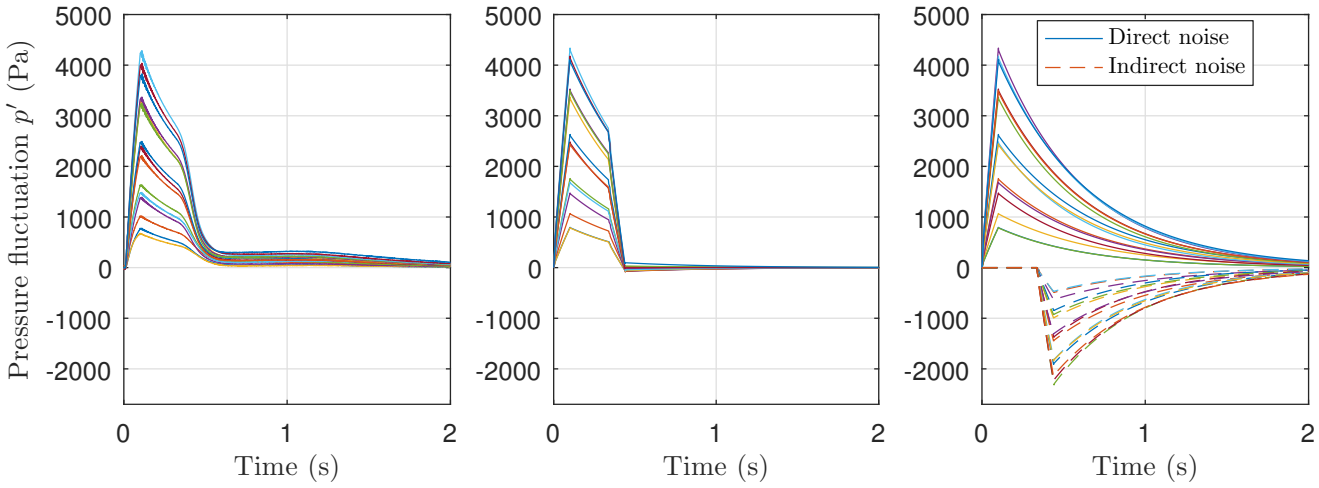

Fig. 12. Experimental acoustic pressure p'_2 (cases B1, B2, B3) for a range of helium flow rates (left), analytical acoustic pressure p' (middle), analytical acoustic pressure contributions of direct(p'_d) and indirect noise (p'_i) (right).

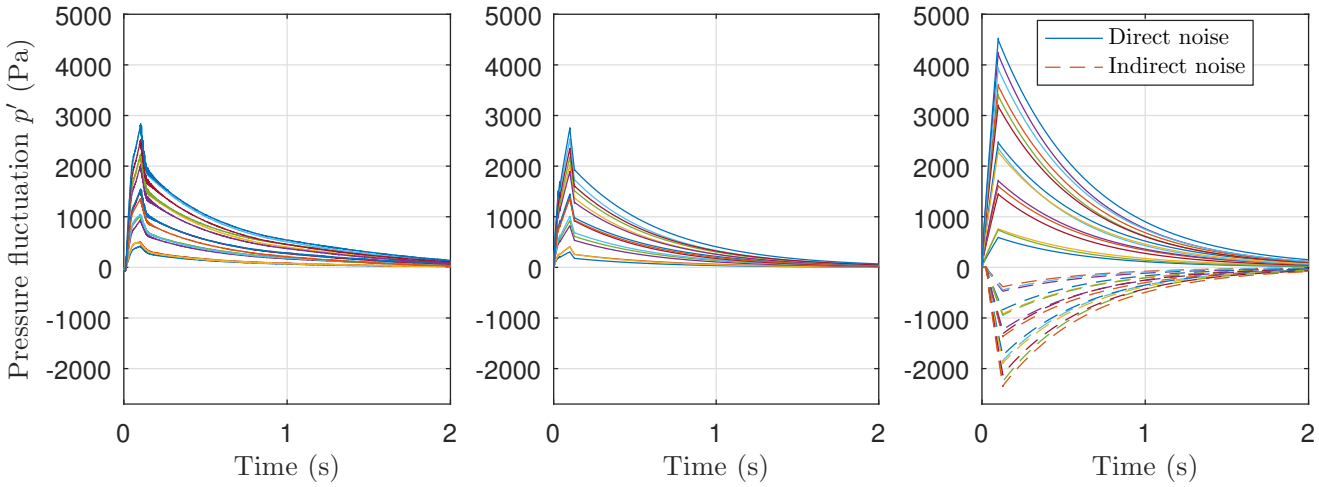

Fig. 13. Experimental acoustic pressure p'_2 (cases C1, C2, C3) for a range of helium flow rates (left) , analytical acoustic pressure p' (middle), analytical pressure contributions of direct (p'_d) and indirect noise (p'_i) (right)

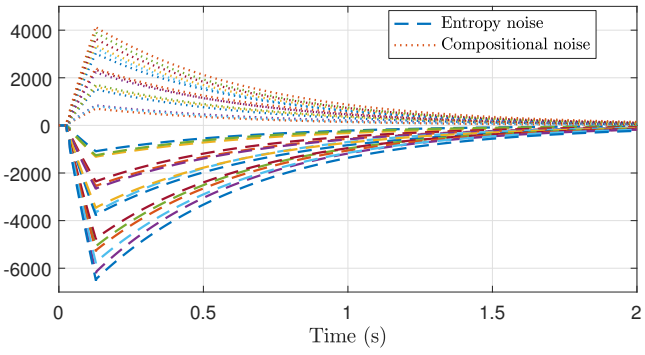

Fig. 14. Entropic (p'_σ) and compositional (p'_ξ) contributions to indirect noise for cases C1, C2, C3.

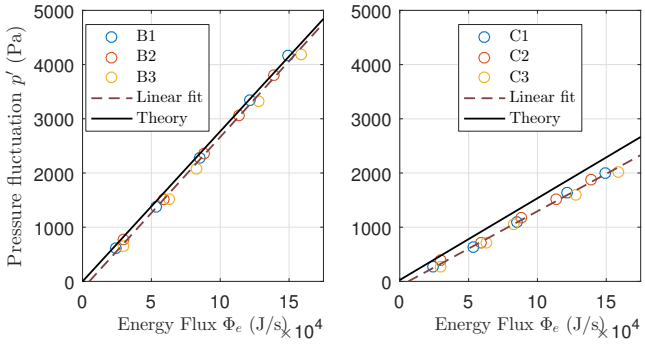

Fig. 15. Comparison of experimental and theoretical peak pressures for direct noise (cases B1, B2, B3, left) and indirect noise (cases C1, C2, C3, right)

noise resulting from the injection and convection of helium disturbances through a choked nozzle. The results of these experiments are compared to an analytical model.

In configuration A, the dimensions of the experimental set-up enable the direct noise to be measured without any indirect noise. As predicted by 1D theory, the direct noise is directly proportional to the amount of helium which is in-

jected. The proportionality coefficient is under-estimated by the analytical model. This discrepancy is attributed to noise sources not taken into account in the 1D model, namely those related to the formation of a jet, vortices, and the effect of a 2D velocity profile.

In configurations B and C, the dimensions of the system are set such that both direct and indirect noise are generated. In addition, the pressure measurements are affected by acoustic reverberation, whereby the acoustic energy accumulates while the acoustic sources are active, and decays exponentially when they are deactivated. A time delay analysis is carried out to identify and separate the contributions of direct and indirect noise to the overall pressure signal. These are then compared directly with the analytical model direct and indirect noise.

The direct noise results are in excellent agreement, which suggests that the reverberation model is accurate. The indirect noise is overestimated in configuration B, but this difference is likely due to helium diffusion and dispersion along the duct (which is not the focus of this study). In configuration C, these effects are not present, and the analytically calculated indirect noise is very close to the experimental result. This suggests that the compact indirect noise transfer functions employed are representative of the behavior of the choked nozzle in the experiment.

While this is not directly visible in the experimental data, analytical results indicate that entropy noise is actually the dominant indirect noise source, while direct and indirect noise are of comparable amplitude for the operating conditions examined here.

Acknowledgements

This work was supported by the UK Engineering and Physical Sciences Research Council (EPSRC) grant EP/K02924X/1. Erwan Rolland is supported by an EPSRC DTA studentship (University of Cambridge), Francesca De Domenico is supported by the Honorary Vice-Chancellor's Award and a Qualcomm / DTA Studentship (University of Cambridge).

References

[1] Dowling, A. P., and Stow, S. R., 2003. "Acoustic Analysis of Gas Turbine Combustors". *Journal of Propulsion and Power,* **19**(5), 9, pp. 751–764.

[2] Strahle, W. C., 1971. "On combustion generated noise". *Journal of Fluid Mechanics,* **49**(02), 9, pp. 399–414.

[3] Marble, F. E., and Candel, S. M., 1977. "Acoustic disturbance from gas non-uniformities convected through a nozzle". *Journal of Sound and Vibration,* **55**(2), pp. 225–243.

[4] Howe, M. S., 2010. "Indirect combustion noise". *Journal of Fluid Mechanics,* **659**, 9, pp. 267–288.

[5] Magri, L., OBrien, J., and Ihme, M., 2016. "Compositional inhomogeneities as a source of indirect combustion noise". *Journal of Fluid Mechanics,* **799**, 7, p. R4.

[6] Morgans, A. S., and Goh, C. S., 2011. "The effect of entropy wave dissipation and dispersion on thermoacoustic instability in a model combustor". In 17th AIAA/CEAS Aeroacoustics Conference (32nd AIAA Aeroacoustics Conference), Portland, OR.

[7] Bohn, M. S., 1977. "Response of a subsonic nozzle to acoustic and entropy disturbances". *Journal of Sound and Vibration,* **52**(2), 5, pp. 283–297.

[8] Cumpsty, N., and Marble, F., 1977. "The Interaction of Entropy Fluctuations with Turbine Blade Rows; A Mechanism of Turbojet Engine Noise". *Proceedings of the Royal Society A: Mathematical, Physical and Engineering Sciences,* **357**(1690), 11, pp. 323–344.

[9] Tao, W., Mazur, M., Huet, M., and Richecoeur, F., 2016. "Indirect Combustion Noise Contributions in a Gas Turbine Model Combustor with a Choked Nozzle". *Combustion Science and Technology,* **188**(4-5), 5, pp. 793–804.

[10] Zukoski, E. E., and Auerbach, J. M., 1976. "Experiments Concerning the Response of Supersonic Nozzles to Fluctuating Inlet Conditions". *Journal of Engineering for Power,* **98**(1), pp. 60–64.

[11] Bake, F., Kings, N., and Roehle, I., 2008. "Fundamental Mechanism of Entropy Noise in Aero-Engines: Experimental Investigation". *Journal of Engineering for Gas Turbines and Power,* **130**(1), p. 11202.

[12] Bake, F., Richter, C., Mühlbauer, B., Kings, N., Röhle, I., Thiele, F., and Noll, B., 2009. "The Entropy Wave Generator (EWG): A reference case on entropy noise". *Journal of Sound and Vibration,* **326**(3-5), 10, pp. 574–598.

[13] Kings, N., and Bake, F., 2010. "Indirect combustion noise: noise generation by accelerated vorticity in a nozzle flow". *International Journal of Spray and Combustion Dynamics,* **2**(3), 9, pp. 253–266.

[14] De Domenico, F., Rolland, E. O., and Hochgreb, S., 2017. "Detection of direct and indirect noise generated by synthetic hot spots in a duct". *Journal of Sound and Vibration,* **394**, 4, pp. 220–236.

[15] Bake, F., Gaetani, P., Persico, G., Neuhaus, L., and Knobloch, K., 2016. "Indirect Noise Generation in a High Pressure Turbine Stage". In 22nd AIAA/CEAS Aeroacoustics Conference, American Institute of Aeronautics and Astronautics.

[16] Mühlbauer, B., Noll, B., and Aigner, M., 2009. "Numerical Investigation of the Fundamental Mechanism for Entropy Noise Generation in Aero-Engines". *Acta Acustica united with Acustica,* **95**(3), 5, pp. 470–478.

[17] Leyko, M., Moreau, S., Nicoud, F., and Poinsot, T., 2011. "Numerical and analytical modelling of entropy noise in a supersonic nozzle with a shock". *Journal of Sound and Vibration,* **330**(16), 8, pp. 3944–3958.

[18] Giauque, A., Huet, M., and Clero, F., 2012. "Analytical Analysis of Indirect Combustion Noise in Subcritical Nozzles". *Journal of Engineering for Gas Turbines and Power,* **134**(11), p. 111202.

[19] Duran, I., Moreau, S., and Poinsot, T., 2013. "Analytical and Numerical Study of Combustion Noise

Through a Subsonic Nozzle". *AIAA Journal,* **51**(1), 1, pp. 42–52.

[20] Lourier, J.-M., Noll, B., and Aigner, M., 2015. "Numerical Investigation of the Entropy Wave Generator Test Case Using Multirate Impedance Boundary Conditions". In 53rd AIAA Aerospace Sciences Meeting, American Institute of Aeronautics and Astronautics.

[21] Becerril, C., Moreau, S., Bauerheim, M., Gicquel, L., and Poinsot, T., 2016. "Numerical investigation of combustion noise: The Entropy Wave Generator". In 22nd AIAA/CEAS Aeroacoustics Conference, American Institute of Aeronautics and Astronautics.

[22] Mühlbauer, B., Noll, B., and Aigner, M., 2009. "Numerical Investigation of the Fundamental Mechanism for Entropy Noise Generation in Aero-Engines". *Acta Acustica united with Acustica,* **95**(3), 5, pp. 470–478.

[23] Rolland, E. O., De Domenico, F., and Hochgreb, S., 2017. "Theory and application of reverberated direct and indirect noise". *Journal of Fluid Mechanics,* **819**, 5, pp. 435–464.

[24] Chu, B. T., and Kovásznay, L. S. G., 1958. "Non-linear interactions in a viscous heat-conducting compressible gas". *Journal of Fluid Mechanics,* **3**(05), 3, pp. 494–514.

[25] Ihme, M., 2017. "Combustion and Engine-Core Noise". *Annual Review of Fluid Mechanics,* **49**(1), 1, pp. 277–310.